Dynamics of the Fragment of Thrombomodulin Containing the Fourth and Fifth Epidermal Growth Factor-like Domains Correlate with Function†

Judith H. Prieto,‡ Benedetta A. Sampoli Benitez,§ Giuseppe Melacini,|| David A. Johnson,⊥ Matthew J. Wood,# and Elizabeth A. Komives*,‡

Department of Chemistry and Biochemistry, University of California, San Diego, La Jolla, California 92093-0378, Departments of Natural Sciences and Mathematics, Marymount Manhattan College, 221 East 71st Street, New York, New York 10021, Department of Chemistry, McMaster University, 1280 Main Street West, Hamilton, Ontario, Canada L8S 4M1, University of California, Riverside, Webber Hall 2130, Riverside, California 92521, and Cell Biology and Metabolism Branch, National Institute of Child Health and Human Development, 18 Library Drive, Building 18T, Room 101, Bethesda, Maryland 20892-5430

Received September 29, 2004; Revised Manuscript Received November 8, 2004

ABSTRACT: Thrombomodulin (TM) forms a 1:1 complex with thrombin. Whereas thrombin alone cleaves fibrinogen to make the fibrin clot, the thrombin−TM complex cleaves protein C to initiate the anticoagulant pathway. The fourth and fifth EGF-like domains of TM together form the minimal fragment with anticoagulant cofactor activity. A short linker connects the fourth and fifth EGF-like domains of TM, and Met 388 in the middle of the linker interacts with both domains. Several different structures of TMEGF45 variants are now available, and these show that mutation of Met 388 alters the structure of the fifth domain, as well as the connectivity of the two domains. To probe this phenomenon more thoroughly, NMR backbone dynamics experiments have been carried out on the individual fourth and fifth domains as well as on the wild type, the Met 388 Leu mutant, and the variant in which Met 388 is oxidized. The results presented here show that changes at Met 388 cause significant changes in backbone dynamics in both the fourth and fifth EGF-like domains of TM. Backbone dynamics within the small loop of the fourth domain Tyr 358 correlate with anticoagulant cofactor activity. Backbone dynamics of the thrombin-binding residues Tyr 413 and Ile 414 are inversely correlated with thrombin binding. The preordering of the backbone of Tyr 413 and Ile 414 only occurs in the two-domain fragments, revealing a role for the fourth domain in thrombin binding as well as in anticoagulant cofactor activity.

Thrombomodulin (TM)[1] is an endothelial cell surface glycoprotein that forms a 1:1 complex with thrombin. When thrombin is in complex with TM, it no longer has procoagulant fibrinogen cleavage activity but instead has new anticoagulant function to activate protein C (*1*). This process is essential for maintenance of hemostasis (*2*, *3*). The 81 amino acid TM fragment composed of the fourth and fifth epidermal growth factor- (EGF-) like domains (TMEGF45) is the smallest active TM fragment (*4*). Although the fifth domain binds to thrombin, anticoagulant cofactor activity requires both the fourth and fifth domains and that they be connected (*4*). Cofactor activity assays and binding kinetic studies have shown that the thrombin−TMEGF45 complex has the same k_{cat} for protein C activation as thrombin−TM but TMEGF45 binds to thrombin 10-fold more weakly than the fragments of TM that also contain the sixth domain (*5*). Met 388 is located in the short three-residue linker between the fourth and fifth EGF-like domains. It is conserved in mouse, bovine, and human TM, and if Met 388 is mutated to any other residue than Leu, the cofactor activity of TM decreases (*6*).

Recent structural studies of TMEGF45 (*7*), the TMEGF456−thrombin complex (*8*), and two mutants, TM45ox and TM45M388L (*9*), reveal the critical importance Met 388 plays in the interaction between the fourth and fifth EGF-like domains of TM. In the structure of TMEGF45, Met 388 is inserted into the fifth domain and has nuclear Overhauser effect (NOE) connectivities to the β carbons of the cysteines that form the disulfide bonds (*7*). In the structure of the fifth domain alone, Met 388 shows no interactions with the domain (*10*). Insertion of Met 388 into the hydrophobic core of the fifth domain may also function to allow exposure of the thrombin-binding residues within this domain. These residues pack against the disulfide bonds in the structure of the fifth domain alone but are exposed in the structure of TMEGF45 (*9*).

The solution structure of TMEGF5 as well as the structure of TMEGF45 shows areas of the protein for which very few NOE connectivities are observed, and the protein structure is therefore not very well determined (*7*, *10*). The structure

† Financial support for this work was provided by NIH Grant RO1-HL070999 to E.A.K. J.H.P. acknowledges support from American Heart Association Fellowship 0110013Y.

* To whom correspondence should be addressed: phone, (858) 534-3058; fax, (858) 534-6174; e-mail, ekomives@ucsd.edu.

‡ University of California, San Diego.

§ Marymount Manhattan College.

|| McMaster University.

⊥ University of California, Riverside.

National Institute of Child Health and Human Development.

[1] Abbreviations: TM, thrombomodulin; EGF, epidermal growth factor; NMR, nuclear magnetic resonance; NOE, nuclear Overhauser effect; CNBr, cyanogen bromide; MALDI-TOF, matrix-assisted laser desorption ionization time of flight.

10.1021/bi0478852 CCC: $30.25
Published on Web 01/07/2005

of the fifth domain from TMEGF45 was even less well determined than that of the fifth domain alone, and fewer NOEs were observed in the fifth domain from the two-domain fragment. This led to the hypothesis that the fourth domain, or the linker, may induce disorder in the fifth domain. One possible explanation for the lack of observed NOEs is that the fifth domain, which has an uncrossed disulfide bonding pattern and no regular secondary structure, may have few interresidue contacts because the three disulfide-bonded loops are "geometrically" separate. In this situation, subtle changes in side chain interactions could alter the conformation of the backbone, and this could explain why the fifth domain structure seemed to be partly disrupted when the fourth domain was attached. Alternatively, the lack of NOEs may truly indicate an increase in backbone flexibility resulting in a situation where the protons are not in a single state long enough for the nuclear Overhauser effect to occur (*11*). To investigate whether flexibility could explain the lack of observed NOEs in the fifth domain of TMEGF45 and whether this flexibility was important for the anticoagulant function of TMEGF45, we decided to perform ^{15}N relaxation studies.

In recent years it has become clear that the biological functions of proteins are related to their dynamic properties. Conformational changes and induced-fit binding phenomena are often invoked to explain biochemical results, but there are few good experimental methods available to actually measure the dynamical behavior of proteins. Nuclear magnetic resonance (NMR) spectroscopy is particular well suited to the investigation of protein dynamics through the measurement of nuclear relaxation times. NMR relaxation experiments can provide information about the dynamic properties of protein backbones and side chains at amino acid resolution on time scales ranging from picoseconds to nanoseconds and from microseconds to milliseconds (*12*−*14*). This makes NMR relaxation experiments an extremely powerful tool that has the potential to bridge the gap between the static picture of macromolecular structures and their biophysical properties such as configurational entropy, hydration, and flexibility, ultimately providing information on how these properties relate to biological function (*15*−*17*).

Heteronuclear NOE measurements of TMEGF45 suggested that the fifth domain is relatively flexible compared to the fourth domain (*7*). Met 388 makes extensive hydrophobic contacts with both the fourth and fifth domains, and we have shown that mutation and oxidation of this residue have large effects on the structure of the fifth domain (*9*). We present here results from ^{15}N relaxation experiments on wild-type TMEGF45, the independent fourth and fifth domains, the overactive M388L mutant, and the variant where Met 388 is oxidized, which together reveal dynamic interactions between the fourth domain and the fifth domain and the role of Met 388 in this interaction.

EXPERIMENTAL PROCEDURES

Preparation of Fluorescently Labeled TMEGF45. TMEGF45 was labeled with two different fluorescein derivatives with different linkers to the protein. Since the protein has no lysine residues, labeling with an amine-reactive probe resulted in a unique product with the fluorophore attached to the N-terminus. The two fluorescent-active labels were 6-(fluorescein 5-carboamido)hexanoic acid succinimidyl ester (FSX) and 5-carboxyfluorescein succinimidyl ester (FAM) (Molecular Probes Inc., Eugene, OR). Coupling was achieved by dissolution of 5 mg of TMEGF45 in 5 mL of 0.5 M sodium bicarbonate, pH 8.3 (pH 9 for the isothiocyanate). Either FSX or FAM was dissolved (10 mg/mL) in 25 mL of DMF and added to the protein solution. After 1 h, the reaction was stopped by adding 0.1 mL of freshly prepared 1.5 M lysine, pH 8.5, and the product was purified by size exclusion chromatography on Superdex 75 FPLC in Tris-buffered saline.

Time-Resolved Fluorescence Intensity and Anisotropy Decay. Samples were excited at 460 nm, and time-resolved emission was determined by the time-correlated single photon-counting technique (*18*) with an EEY scientific nanosecond spectrofluorometer (La Jolla, CA) equipped with an IBH (Edinburgh, U.K.) hydrogen-arc flash lamp as described in more detail in Hauer et al. (*19*). The fluorescence intensity decay $I(t)$ was analyzed as a sum of decaying exponentials with each ith term having a lifetime τ_i and an amplitude α_i (eq 1). Anisotropy decay measurements were

$$I(t) = \Sigma_i \alpha_i \exp(t/\tau_i) \quad (1)$$

performed by acquiring the time-dependent vertically and horizontally polarized fluorescence intensity decays [$I_{||}(t)$ and $I_{\perp}(t)$, respectively] when excited by vertically polarized light, using a multichannel plate detector (*19*). Using the Globals Unlimited Software package [Laboratory of Fluorescence Dynamics, Urbana, IL (*20*)] the data were then analyzed by fitting $I_{||}(t)$ and $I_{\perp}(t)$ according to eqs 2 and 3. The time-

$$I_{||}(t) = (1/3)I(t)[1 + 2r(t)] \quad (2)$$

$$I_{\perp}(t) = (1/3)I(t)[1 - r(t)] \quad (3)$$

dependent anisotropy decay $r(t)$ fit well to a biexponential equation with fast (F) and slow (S) processes (eq 4).

$$r(t) = r_F \exp(-t/\phi_F) + r_S \exp(-t/\phi_S) \quad (4)$$

Preparation of ^{15}N-Labeled Proteins. The uniformly ^{15}N-labeled single domains TMEGF4 (residues Glu 346−Met 388) and TMEGF5 (residues Phe 389−Glu 426) were obtained from CNBr cleavage of a mutant TMEGF45 protein in which another methionine was inserted next to Met 388 that was expressed in *Pichia pastoris*. The insertion of the second methionine resulted in much higher yields of cleaved products. It has been previously shown that the smallest active fragment of TM is TMEGF45, and cleavage into the individual domains causes a complete loss of cofactor activity (*4*). However, binding of the fifth domain to thrombin can still be assessed, and this assay was used to monitor purity of the resulting fifth domain fragment (*21*). Fermentation of the *P. pastoris* to produce this double Met mutant and the subsequent protein purification were carried out as described before (*22*). CNBr cleavage was carried out overnight at 37 °C in 70% formic acid with approximately 50% efficiency. The two single domains were then further purified from the remaining two-domain fragment by chromatography on a MonoQ (5/5) column (Amersham Biosciences, Piscataway, NJ). The fourth domain did not stick to the column, while the fifth domain could be separated from uncleaved double

Met-TMEGF45 using a linear gradient from 0 to 1 M NaCl with 50 mM Tris buffer at pH 7.5. Approximately 0.6 mg of each of the purified domains was produced per liter of fermentation. Molecular masses of products were determined by MALDI-TOF mass spectrometry after endoglycosidase H treatment (*4*) and were 5128 Da for TMEGF4 and 4363 Da for TMEGF5. The mass spectrometric analysis revealed only one cleavage after the second methionine had occurred. Thus, the resulting fourth domain fragment retained a single methionine at the C-terminus, while the resulting fifth domain fragment began with phenylalanine. The wild-type protein and mutants TMEGF45M388ox and TMEGF45M388L were obtained as described previously (*7*, *9*, *22*).

NMR Spectroscopy. NMR samples were 0.25 mM for the single domains and between 0.8 and 1 mM for the two-domain proteins, in 90% H_2O/10% D_2O with 2 mM NaN_3, pH 6.5. All experiments were collected at 310 K on a Bruker DRX600 or a Bruker DMX500 operating at 600.13 and 500.13 MHz, respectively, with a 5 mm triple resonance probe and pulsed field gradient units. The pulse schemes used to measure R_1, R_2, and the $\{^1H\}-^{15}N$ NOE were from Farrow et al. (*23*) modified for Bruker by John Chung, TSRI (*23*). All of the experiments were performed using 2 ms water flip-back pulses for minimum water saturation and employed gradients for coherence selection (*23*).

The R_1 and R_2 experiments were recorded in duplicate. Values of the longitudinal relaxation rates (R_1) for each amide were measured from the spectra recorded with seven different delay times: $t = 20$, 40, 80, 160, 320, 640, and 1280 ms. Values of the transverse relaxation rate (R_2) for each amide were obtained from spectra recorded with eight different delay times: $t = 10$, 20, 40, 60, 80, 120, 160, and 320 ms. All of the data sets were collected with 1024 × 256 complex data points and 16 scans for the two-domain fragments and 32 scans for the single domains. The receiver gain was set for all experiments to 1024. Data were processed using Felix 98 (Molecular Simulations Inc., San Diego, CA) to a final matrix size of 1024 × 512 points.

Values of the $\{^1H\}-^{15}N$ steady-state NOE for each amide were determined by recording spectra in the presence and absence of a proton presaturation period of 3 s. Saturation of the ^1H nuclei was achieved with the use of 120° ^1H pulses applied every 5 ms (*24*). Each NOE experiment was run in duplicate in order to evaluate the signal-to-noise ratio and the reproducibility of peak intensities. Heteronuclear NOE experiments were collected with 512 × 256 complex points and 48 transients at 600 MHz and with 512 × 128 and 48 transients at 500 MHz. For the single domains 96 transients were collected. Data were processed using Felix 98 (Molecular Simulations Inc.) to a final matrix size of 512 × 256.

The experiments to measure η_{xy}/η_z were carried out using pulse sequences adapted from Kroenke et al. (*25*, *26*). The η_{xy} were measured using delays times of 32, 53.4, 74.8, 96.1, and 106.8 ms. The η_z were measured using delay times of 150, 225, 300, 375, and 450 ms. Each NMR experiment was collected with 1024 × 256 complex data points. Both the η_{xy} and η_z measurements involve running an experiment with the dipolar/CSA cross-relaxation term (I_{cross}) and an experiment without it (I_{auto}), for each delay time. For both cross-relaxation experiments, 64 scans were collected in experiments used to measure I_{cross}, and 16 scans were collected to measure I_{auto}.

NMR Analysis. The ^{15}N relaxation data were analyzed using the reduced spectral density function mapping as described in detail elsewhere (*27*−*29*). In the reduced spectral density function approach, one assumes that $dJ(\omega)/d\omega^2$ is relatively constant between the linear combinations ($\omega_H + \omega_N$) and ($\omega_H - \omega_N$). The rate constants and NOE can then be expressed as a linear combination of only three spectral density functions, $J(0)$, $J(\omega_N)$, and $J(0.87\omega_H)$ (*27*−*30*). Following this procedure, the spectral density functions at these three frequencies can be written in terms of the relaxation parameters (eqs 5−7)

$$J(0) = (6R_2 - 3R_1 - 2.72\sigma)/(3d^2 + 4c^2) \quad (5)$$

$$J(\omega_N) = (4R_1 - 5\sigma)/(3d^3 + 4c^2) \quad (6)$$

$$J(0.87\omega_H) = 4\sigma/5d^2 \quad (7)$$

where $\sigma = [(\mathrm{NOE} - 1)R_1\gamma_N/\gamma_H]$ is the cross-relaxation rate of the spin pair, $d = [\mu_o h\gamma_H\gamma_N/8\pi^2]\langle r_{NH}^{-3}\rangle$ and $c = \omega_N\Delta\sigma/\sqrt{3}$, μ_o is the permeability of free space, h is Planck's constant, γ_H and γ_N are the gyromagnetic ratios of the ^1H and ^{15}N nuclei, respectively, ω_H and ω_N are the Larmor precessional frequencies of the ^1H and ^{15}N nuclei, r_{NH} is the nitrogen−hydrogen bond length (1.02 Å), and $\Delta\sigma$ is the chemical shift anisotropy of the ^{15}N spins (−160 ppm) (*31*).

Accurate estimation of $J(0)$ values is complicated because the measured R_2 values are sensitive to motions on the millisecond to microsecond time scale. These motions tend to increase the apparent values of $J(0)$ and may yield unreliable estimates of $J(0)$ in some cases. As the contributions of these motions to the effective line width increase with the square of the spectrometer frequency, measurements at two field strengths (500 and 600 MHz) allow the determination of reliable effective spectral density values close to the zero frequency $J_{eff}(0)$ (*28*):

$$J_{eff}(0) = 1/\beta\{(R_2^{600} - \kappa R_2^{500}) - (3d^2/8)[J(\omega_N^{600}) - \kappa J(\omega_N^{500})] - (c_2^{600}/2)[J(\omega_N^{600}) - J(\omega_N^{500})] - (13d^2/8)[J(0.955\omega_H^{600})\kappa J(0.955\omega_H^{500})]\} \quad (8)$$

where $\kappa = (\omega_H^{600}/\omega_H^{500})^2$, $\beta = (1 - \kappa)d^2/2$, and the subscripts and superscripts denote the frequency of the spectrometer at which the measurements were performed.

Accurate estimation of motions on the microsecond to millisecond time scale, known as chemical exchange (R_{ex}), is critical for correct interpretation of spectral density mapping results. Residues that have significantly elevated R_2/R_1 ratios have been shown to have contributions from R_{ex} (*32*). Also, if the molecule is tumbling anisotropically, the R_2/R_1 ratio can increase and be mistaken for R_{ex} contributions (*26*). To determine if large R_2/R_1 ratios result from R_{ex} or anisotropic behavior, Kroenke et al. developed methods that can measure the longitudinal cross-correlation relaxation rate constant (η_z) for $^1H-^{15}N$ dipolar/^{15}N chemical shift anisotropy (CSA) relaxation interference (*25*). Combined with the transverse cross-correlation relaxation rate constant (η_{xy}), the ratio of η_{xy}/η_z is sensitive to the internal and overall motions that contribute to the dipolar and CSA relaxation mechanisms. Since η_{xy}/η_z is independent of R_{ex} contributions, comparison with R_2'/R_1' ratios allows for identification of

^{15}N nuclei that undergo R_{ex} processes. R_1' and R_2' are the modified relaxation rates that have the high-frequency components of local motion subtracted out according to eqs 9 and 10 (*25*).

$$R_1' = R_1 - 1.249\sigma \quad (9)$$

$$R_2' = R_2 - 1.079\sigma \quad (10)$$

Data Analysis. Relaxation rate constants and heteronuclear NOEs were calculated from cross-peak heights in the ^{1}H−^{15}N correlation spectra. Peak heights were measured from the NMR spectra using routines written in the Felix macro programming language (Copyright 1994, Mikael Akke). Assignments for the peaks for the fifth domain were confirmed with NOESY and TOCSY experiments. The longitudinal relaxation times, T_1, were obtained by a three-parameter (I_∞, I_0, and T_1) nonlinear least-squares fit of eq 11 to the experimental data:

$$I(t) = I_\infty - (I_\infty - I_0)\exp(-t/T_1) \quad (11)$$

The transverse relaxation times, T_2, were obtained by a two-parameter (I_0 and T_2) nonlinear least-squares fit of the experimental data to the equation:

$$I(t) = I_0\exp(-t/T_2) \quad (12)$$

where I_0 and I_∞ are the initial and final cross-peak heights, respectively. Curve fitting was done using the Levenburg−Marquardt algorithm implemented in the program CURVEFIT (Copyright 1998, Arthur G. Palmer) (*33*, *34*).

{^{1}H}−^{15}N steady-state NOE (hNOE) were calculated from two data sets according to the equation:

$$\text{hNOE} = I_{sat}/I_{unsat} \quad (13)$$

in which I_{sat} and I_{unsat} are the peak intensities in spectra recorded with and without saturation of protons during the recycle delay.

For the cross-correlation experiments, the peak intensities for I_{cross} and I_{auto} were measured using Felix 97.0 macros after each data set was normalized for the number of scans recorded. The cross-peak intensity ratios I_{cross}/I_{auto} were determined in the same manner as I_{sat}/I_{unsat} for hNOE experiments. The I_{cross}/I_{auto} ratios were plotted against the delay times (τ), and η_{xy} or η_z was calculated by nonlinear least-squares fitting to the hyperbolic tangent functions (eqs 14 and 15) using CURVEFIT.

$$I_{cross}/I_{auto} = \tanh(\eta_{xy}\tau) \quad (14)$$

$$I_{cross}/I_{auto} = \tanh(\eta_z\tau) \quad (15)$$

RESULTS

Molecular Tumbling of Wild-Type TMEGF45. The time-resolved anisotropy decay fit well to a biexponential equation, and the anisotropy decay profiles for the FAM and FSX derivatives each showed a "fast" and a "slow" decay process. The slow decay process gives ϕ_S, which corresponds to the whole-body rotational correlation time of the molecule. With either fluorescent probe, the rotational correlation time was 6−7 ns, consistent with a monomer molecular mass for TMEGF45 of 9.4 kDa when the protein was dissolved in water (Supplementary Table 1; see Supporting Information). When TMEGF45 was dissolved in a buffered solution, much higher correlation times (18−21 ns) were obtained, indicating aggregation or dimerization. Similar results were obtained from analytical ultracentrifuge experiments under several buffer and pH conditions (data not shown). On the basis of these results, all NMR experiments were carried out in H_2O. These results were taken to indicate that the TMEGF45 molecule was not highly anisotropic in its tumbling behavior despite the elongated shape of this two-EGF-like domain fragment. This is probably due to the two relatively large N-linked glycans, one on the fourth domain and one on the fifth domain.

Backbone Dynamics of Wild-Type TMEGF45. TMEGF45 is an 82-residue protein, but there are 9 proline residues, so the total possible observable backbone amide resonances is 72. Relaxation rates R_1 and R_2 were measurable for 60 of the backbone amide resonances. Cross-peaks for residues Asp 416, His 381, and Thr 422 were not visible, cross-peaks for Gln 365, Cys 390, Gln 392, Ala 394, Asp 423, and Ile 424 were too weak to allow a reliable calculation of the relaxation rates, and cross-peaks for residues Arg 353 and Ser 367 were overlapped and their heights could not be measured accurately. We observed several cross-peaks of varying intensity that appeared to correspond to Ser 406, and therefore we do not report any relaxation data for this residue. Heteronuclear NOE data were measurable for 60 residues because cross-peaks were too weak for Ala 377 and Gly 412; however, a cross-peak for Gln 365 was visible and better resolved in the hNOE spectra than in the R_1 or R_2 relaxation spectra. In certain cases, where the peak intensities were more or less equivalent for all of the peaks belonging to the same spin system (i.e., Met 388, Asp 417, and Glu 408), the relaxation rates of the individual peaks were calculated, and then the final values were averaged.

Inspection of the relaxation data at both 500 and 600 MHz immediately reveals some interesting features about this protein fragment. Figure 1 summarizes the R_1 and R_2 and hNOE data collected at 500 and 600 MHz. The R_1 values were more or less homogeneous for all residues in the protein. The average value for R_1 was 1.5 s^{-1} and ranged from 0.9 to 1.7 s^{-1} for the ordered residues. As expected, the values for R_1 measured at 500 MHz were larger than the values measured at 600 MHz for most residues. Dramatic differences between the fourth and fifth domains appeared in the R_2 and hNOE values for TMEGF45. Overall, values of R_2 and hNOE for the fourth domain were much higher than those for the fifth domain. Taken together, these data suggest that the fifth domain of TM is flexible with motions on the nanosecond time scale.

It was also possible that the higher R_2 values within the fourth domain were due to R_{ex} contributions. To address this issue, the cross-correlation relaxation rate constants (η_{xy} and η_z) for ^{1}H−^{15}N dipolar/^{15}N CSA relaxation interference were measured. The relaxation constants η_{xy} and η_z are not influenced by R_{ex}. Therefore, amide bonds that have contributions from R_{ex} will have an R_2'/R_1' ratio that is greater that their η_{xy}/η_z ratio. Residues that have a R_{ex} contribution fall to the right side of the diagonal and include Gln 361, Val 371, and Thr 366 in the fourth domain and Gly 412, Thr 393, and Asp 400 in the fifth domain (Figure 2). Since

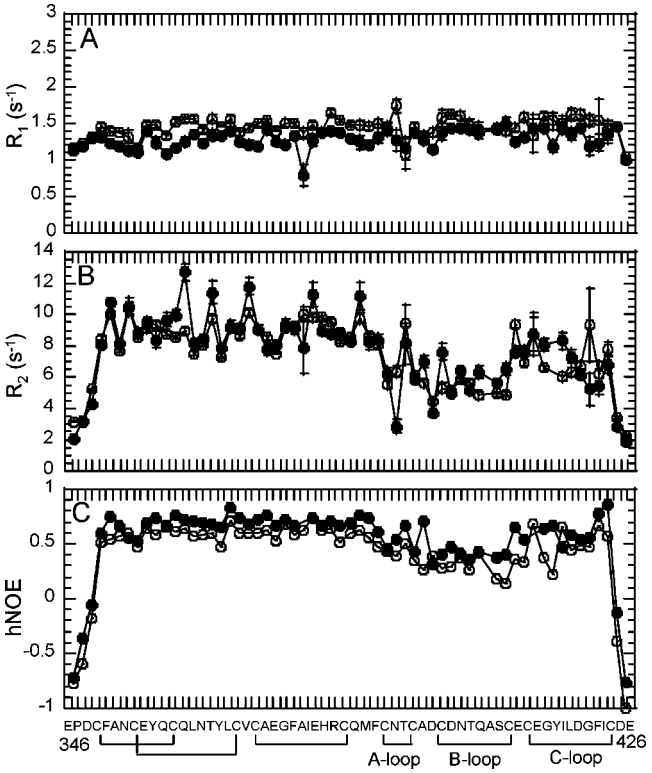

FIGURE 1: Plots of R_1, R_2, and hNOE as a function of residue at 500 MHz (open circles) and 600 MHz (filled circles) for wild-type TMEGF45. (A) R_1 values. (B) R_2 values. (C) $\{^1H\}-^{15}N$ NOE values.

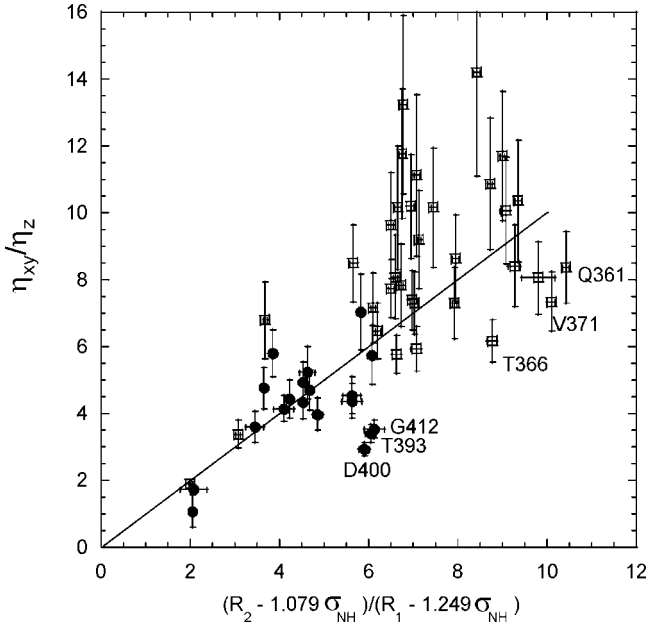

FIGURE 2: Comparison of η_{xy}/η_z and R_2'/R_1' ratios for TMEGF45 measured according to Kroenke et al. To allow for quantitative comparison, the high-frequency components of R_2/R_1 were subtracted out using eqs 12 and 13 to give R_2'/R_1'. Open squares represent residues in the fourth domain, and closed circles denote fifth domain residues.

there were an equal number of residues in each of the domains that have R_{ex} contributions, the differences between the R_2 values measured for the fourth domain and fifth domain could be attributed to faster internal motions on the picosecond to nanosecond time scale within the fifth domain.

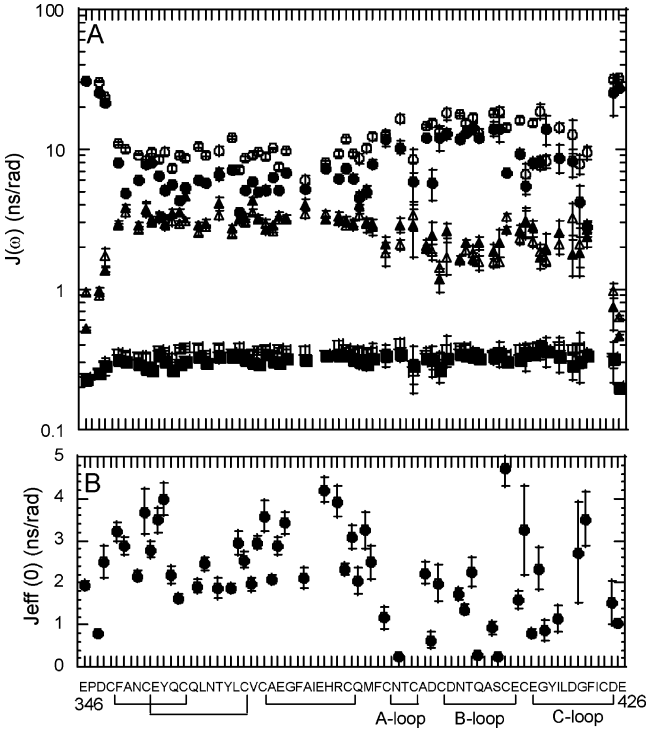

FIGURE 3: (A) Logarithmic plot of the spectral density function of TMEGF45 (ns/rad) obtained at different frequencies: 0 (open triangles, 500 MHz; filled triangles, 600 MHz), $J(\omega_N)$ 50 MHz (open squares) and 60 MHz (closed squares), and $J(0.87\omega_H)$ 438 MHz (open circles) and 540 MHz (filled circles). (B) Effective spectral density close to zero frequency [$J_{eff}(0)$] for TMEGF45 estimated using reduced spectral density mapping at two spectrometer field strengths (500 and 600 MHz).

Reduced spectral density mapping was used to establish the range of motions for each of the proteins. The effective spectral density close to zero frequency, $J_{eff}(0)$, was calculated from the hNOE, the R_1 rate, and the R_2 rates (eq 8) obtained at 500 and 600 MHz. The trend for $J(0)$ (Figure 3) was very similar to the trend observed for the R_2 rates and to some extent to the hNOEs. The average $J_{eff}(0)$ for the fifth domain was 1.92 ± 0.46 ns/rad, and the average $J_{eff}(0)$ for the fourth domain was 2.65 ± 0.26 ns/rad. It can also be seen that a portion of the fifth domain, corresponding to the C-loop (residues Cys 409−Cys 421), has $J_{eff}(0)$ values more similar to the fourth domain (Figure 3).

Differences in Dynamics between the Single Domains and the Two-Domain Pair. The relaxation rates of the single domains have been compared to those observed for the two-domain TMEGF45. R_1 values were somewhat higher for the individual domains than for the two-domain fragment, and this is likely because of the differences in molecular masses (Figure 4). For each of the individual TMEGF domains, R_1 was relatively constant. The difference in the average rates when the domains are compared to each other may indicate a weak association could be taking place in the TMEGF4 sample even at its low 0.25 mM total concentration in the NMR tube. The R_2 values for the single domains were lower than for TMEGF45, consistent with the difference in expected tumbling time. The effective spectral density at frequency zero, $J_{eff}(0)$, calculated from the data obtained at 500 and 600 MHz for the individual domains again mirrored the raw R_2 and hNOE data (data not shown). The main difference between the single domains and the two-domain

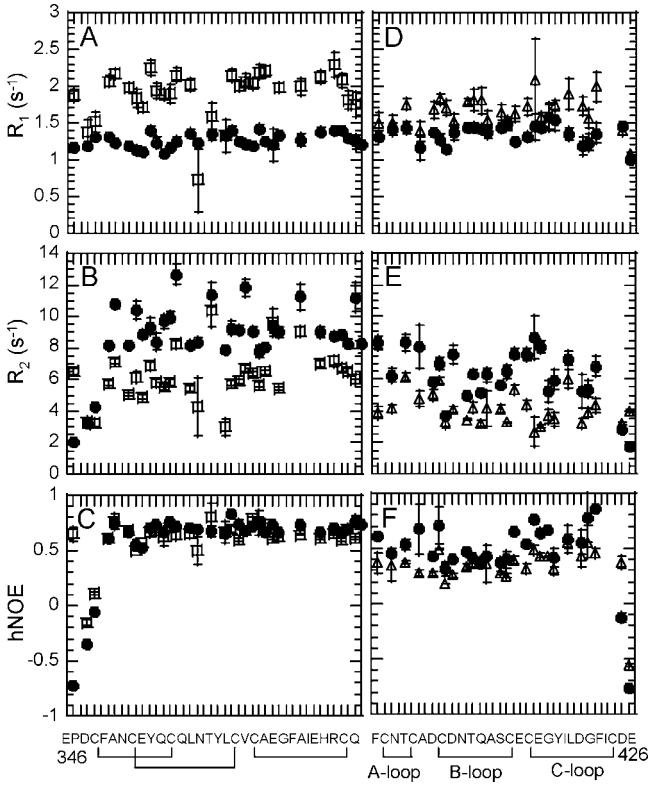

FIGURE 4: Plots of (A) R_1, (B) R_2, and (C) hNOE for the single domain TMEGF4 (open squares) and (D) R_1, (E) R_2, and (F) hNOE for the single domain TMEGF5 (open triangles) compared to the corresponding domain from the two-domain wild-type TMEGF45 (filled circles) at 600 MHz for the 61 residues covered in the analysis.

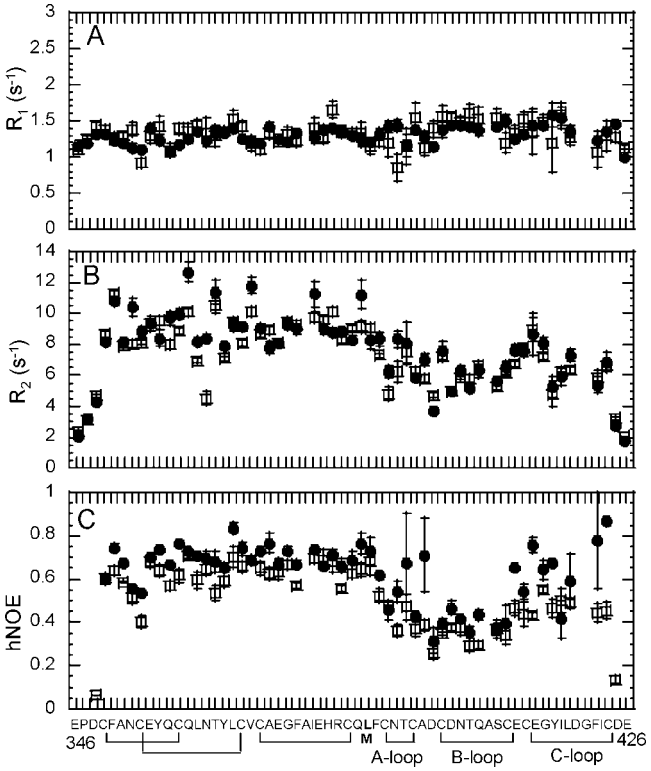

FIGURE 5: Plots of (A) R_1, (B) R_2, and (C) hNOE for the mutant TMEGF45M388L (open squares) compared to wild-type TMEGF45 (filled circles) at 600 MHz for the 61 residues covered in the analysis.

fragment was that the R_2 values of the fifth domain alone were all nearly the same, whereas in the two-domain fragment, the R_2 values of the C-loop (Cys 409−Cys 421) were significantly higher than the R_2 values for the A- and B-loops. In fact, the R_2 values for Tyr 413−Asp 417 were some of the lowest in the single domain, TMEGF5. Thus, the presence of the fourth domain may be imparting order in the C-loop of the fifth domain in the two-domain fragment.

Relaxation studies were also carried out after the fourth domain was treated with endoglycosidase H, which cleaves off the mannoses added by the yeast posttranslational modification machinery and leaves a single GlcNac attached to the asparagine. The relaxation rates of the TMEGF4 with and without sugars were virtually the same (data not shown). Differences were only observed for the glycosylation site residue, Asn 364, confirming that the high mannose glycosylation does not affect the relaxation rates of the rest of the domain. Asn 364, which is glycosylated in both TMEGF4 and TMEGF45, showed much lower R_1, R_2, and hNOE values in TMEGF4 compared to TMEGF45. This may be explained in part by the observation of NOEs between the GlcNAC on the fourth domain and residues within the fifth domain, suggesting an intramolecular interaction that may stabilize the glycosylation site in the two-domain fragment (*7*).

Changes in Dynamics upon Substitution of Met 388. In general, the dynamic properties for the superactive TMEGF45M388L mutant were very similar and follow the same trends as the wild type (Figure 5). Slight differences were observed in the relaxation rates within the C-loop of the fifth domain so that Cys 409, Tyr 413, and Asp 417 had slightly lower R_2 values than the corresponding residue in the wild-type protein (Figure 5B). Lower values of the hNOEs were also observed for these residues and Cys 411, Gly 412, Ile 414, Ile 420, and Cys 421. The N-terminal residues of the fourth domain, residues Glu 357, Tyr 358, and Gln 359, had lower hNOE values perhaps indicative of a slight increase in backbone mobility of this fourth domain loop in the M388L mutant (Table 1).

Table 1: Relaxation Data for Essential TM Residues

residue	TM variant	R_2	hNOE
fourth domain			
Glu 357	wild type	9.3 ± 0.5	0.70 ± 0.015
	Met388Leu	9.3 ± 0.3	0.68 ± 0.03
	Met388ox	9.7 ± 0.2	0.71 ± 0.001
Tyr 358	wild type	8.4 ± 0.5	0.74 ± 0.01
	Met388Leu	9.5 ± 0.3	0.64 ± 0.03
	Met388ox	10.0 ± 0.2	0.79 ± 0.07
Gln 359	wild type	9.7 ± 0.4	0.66 ± 0.001
	Met388Leu	8.0 ± 0.3	0.57 ± 0.02
	Met388ox	9.2 ± 0.1	0.61 ± 0.01
fifth domain			
Tyr 413	wild type	8.0 ± 0.4	0.64 ± 0.04
	Met388Leu	7.2 ± 0.2	0.55 ± 0.02
	Met388ox	3.5 ± 0.01	0.27 ± 0.01
Ile 414	wild type	5.2 ± 0.7	0.67 ± 0.01
	Met388Leu	4.8 ± 0.8	0.47 ± 0.04
	Met388ox	4.1 ± 0.1	0.36 ± 0.02

Oxidation of Met 388 to produce TMEGF45M388ox results in changes within the C-loop of the fifth domain. When Met 388 is oxidized, the B- and C-loops of the fifth domain appeared more motional with significantly lower R_2 values measured for Asp 400, Thr 403, Ala 405−Glu 408, Gly 412, Tyr 413, Ile 414, Asp 417, and Ile 420 (Figure

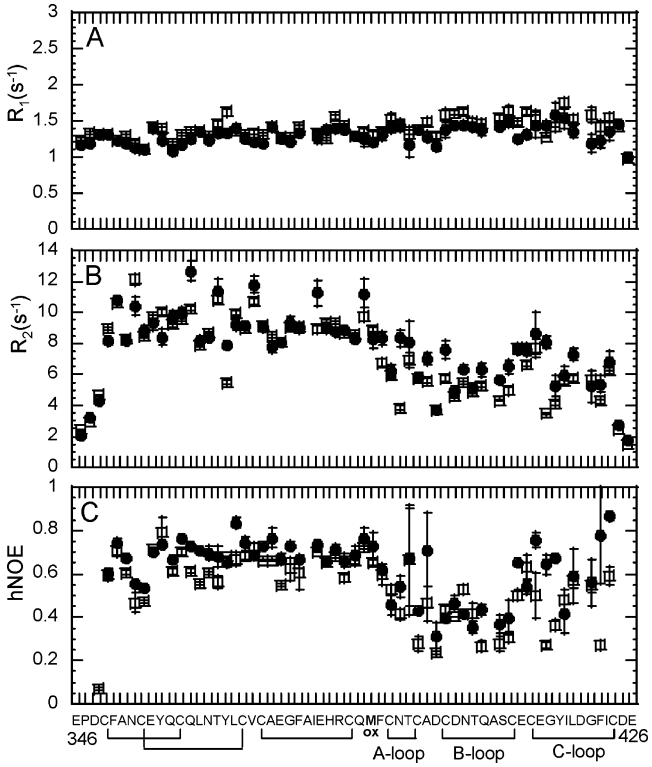

FIGURE 6: Plots of (A) R_1, (B) R_2, and (C) hNOE for TMEGF45ox (open squares) compared to wild-type TMEGF45 (filled circles) at 600 MHz for the 61 residues covered in the analysis.

6B). The hNOEs were significantly lower than in the wild-type protein for residues Ala 405−Glu 408, Gly 412, Tyr 413, and Ile 414 (Figure 6C). Again, decreases in R_2 and hNOE values were reflected in decreased values of $J_{eff}(0)$ calculated from the data obtained at 500 and 600 MHz (data not shown). Importantly, the rise in R_2 and hNOE values that was seen for the wild-type TMEGF45 was not seen for the protein when Met 388 was oxidized. As for the fifth domain alone, the values of R_2 and hNOE were relatively constant throughout the fifth domain and lower than in the fourth domain (Figure 6).

DISCUSSION

Backbone Dynamics of Wild-Type TMEGF45. The smallest fragment of TM that has full anticoagulant cofactor activity is TMEGF45. This fragment binds to thrombin 10-fold more weakly than TMEGF456, but we have shown previously that the sixth domain does not contribute to promotion of protein C activation (*4*). A study of the backbone dynamic properties of TMEGF45 was therefore likely to recapitulate dynamic properties of full-length TM that relate to its anticoagulant activity. Indeed, the dynamic properties of this nonglobular cofactor protein reveal several interesting features. First, the linker between the two domains in two-domain fragments typically has the highest mobility, and this is not the case for TMEGF45. The linker residues are highly ordered in all cases, even when the linker Met 388 is oxidized. Second, the tumbling properties as well as the R_2 values are most consistent with the two domains tumbling as a single unit rather than as two independent domains. Third, comparison of the relaxation properties of the fourth domain (typical, crossed disulfide bonds) and the fifth domain (atypical uncrossed disulfide bonds) shows that the uncrossing of the disulfide bonds increases the backbone mobility of the entire fifth domain, but particularly the A- and B-loops which contain the anomalous disulfide bonds.

In the two-domain fragment, TMEGF45, the C-loop of the fifth domain was markedly more ordered than in the fifth domain alone. Thus, the presence of the fourth domain promotes order in the C-loop of the fifth domain. This conclusion is surprising because we actually observed fewer long-range NOEs in the C-loop of the fifth domain when the fourth domain was present. This effect is probably indirect because no long-range NOEs were observed between fourth domain and fifth domain residues; instead NOEs were observed between Phe 376 and Met 388 and between Met 388 and the fifth domain disulfide bonds (*7*). When one compares the few long-range NOEs observed for the fifth domain, one can see that, in the case of the fifth domain alone, Tyr 413, Ile 414, and Leu 415 were packed against the disulfide bonds and this was not the case for the fifth domain in the context of the fourth. Thus, subtle changes in side chain interactions among the three separately disulfide-bonded loops resulted in more long-range NOEs being observed in the single fifth domain. These side chain interactions did not impart more backbone order; in fact, these residues had higher mobility in the fifth domain alone than in the two-domain fragment. Conversely, in TMEGF45, insertion of Met 388 into the core of the fifth domain results in fewer long-range NOEs from the side chains of residues in the C-loop, but greater backbone order. Thus, the fifth domain of TM represents a case where the number of long-range NOEs is not a good indicator of backbone order, and relaxation studies are absolutely essential. This is most likely because the fifth domain has a pliable three-loop structure in which subtle changes in side chain or backbone interactions cause significant changes in structure (*9*). These structural changes are apparently associated with unpredictable changes in backbone mobility.

Dynamical Changes upon Variation of the Linker Met 388. Two different variants of TMEGF45 were studied, TMEGF45M388L and TMEGF45M388ox. The backbone relaxation properties of the M388L mutant differed from the wild-type protein in both the fourth and fifth domains (Figure 7). In the fourth domain, significantly lower values of the hNOE were observed for Tyr 358 and Gln 359. It is interesting to speculate that the increased mobility in these residues that are essential for anticoagulant cofactor activity may correlate with the improved k_{cat} for protein C activation of the M388L mutant. In the fifth domain, significantly lower values were observed for residues Gly 412, Tyr 413, Ile 414, Ile 420, and Cys 421 (Figures 5 and 7B). These differences correlate with differences in the structure of the fifth domain due to the substitution of Met 388 with Leu. Unlike the methionine, which interacts with all three cysteine disulfide bonds in the fifth domain, the branched leucine side chain only interacts with the disulfide bonds from the A- and B-loops but not with Cys 411 and Cys 421 of the C-loop.

Oxidation of Met 388 has marked consequences on the backbone dynamics of TMEGF45. Residues Ser 406, Cys 407, Glu 408, Gly 412, Tyr 413, and Ile 414 all have lower values of R_2 and hNOE and, consequently, lower $J_{eff}(0)$ values in the oxidized protein (Figures 6 and 7C). The average across the fifth domain is 1.5 ± 0.2, which is closer to the average for the $J_{eff}(0)$ values for the single fifth domain

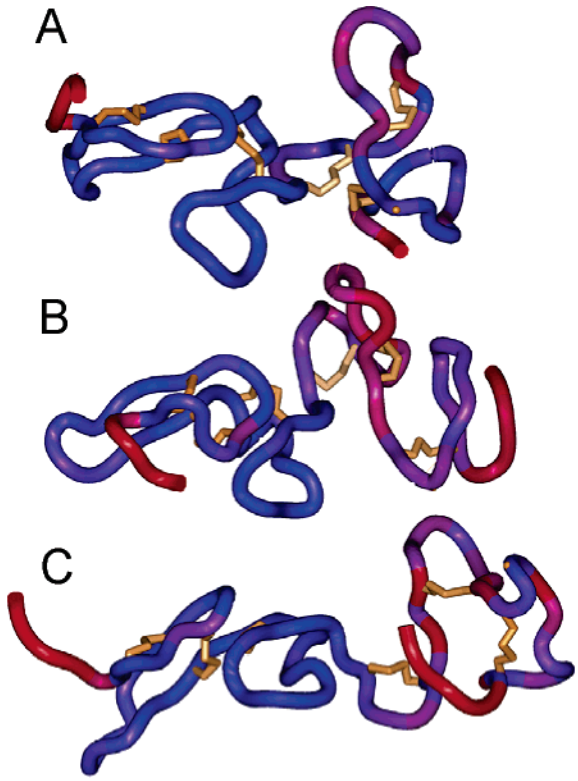

FIGURE 7: Backbone ribbon of the lowest energy structure from the ensemble of structures of (A) wild-type TMEGF45, (B) TMEGF45M388L, and (C) THEMG45M388ox colored according to the heteronuclear NOE values with blue being the highest and red being the lowest.

than for the fifth domain in the two-domain fragment. Thus, oxidation of Met 388 appears to uncouple the two domains, causing them to have backbone dynamics similar to the individual domains. This result confirms that the linker Met serves as a critical connection between the fourth and fifth domains of TM.

Correlation of Dynamics with Anticoagulant Cofactor Activity. Within the fourth domain, Glu357 and Tyr358 are essential for anticoagulant cofactor activity. In the structural analysis of the M388L mutant, we observed NOEs between Phe 376 and Tyr 358 that were not observed in the wild-type protein. This observation suggested a side chain pathway from the residues essential for anticoagulant cofactor function to the fifth domain residues essential for thrombin binding (*9*). The backbone dynamics measurements show that residues Tyr 358 and Gln 359 are significantly more mobile in the M388L mutant than in either the wild type or the methionine oxidized variant. In this case also, it appears that new side chain NOE interactions between aromatic residues result in increased backbone mobility rather than decreased backbone mobility. It is also interesting that these are precisely the residues that are essential for k_{cat} for protein C activation (E. Komives, unpublished data). Thus, it appears that cofactor activity may correlate with backbone flexibility of the essential residues within the fourth domain.

Correlation of Dynamics with Thrombin Binding. Nearly all of the resonances within the fifth domain of TMEGF45 showed chemical shift perturbation upon binding to thrombin, suggesting an induced-fit mechanism of binding (*7*). Our hypothesis was that dynamics within the fifth domain of TM might be important for thrombin-binding function (*7*). This has been observed in other systems such as the phosphotransferase Spo0F and the SH2 domains of phospholipase Cγ1 (*13*, *35*). Within the fifth domain, residues Tyr 413 and Ile 414 are essential for thrombin binding, and mutation of either of these residues to alanine results in complete loss of thrombin-binding function (*36*). The hNOEs and R_2 values for these residues were highest in the wild-type TMEGF45, somewhat lower in the TMEGF45M388L, and lowest in the Met388ox variant (Table 1). In fact, the low hNOE and R_2 values observed in the M388ox variant were similar to those in the individual fifth domain. It is interesting that, in the individual fifth domain and in the M388ox variant, we observe high backbone mobility for Tyr 413 and Ile 414, and these are the variants in which NOEs indicate that these side chains are packed against the disulfide bonds. These are also the variants for which thrombin binding is impaired. In the M388L and wild-type proteins that bind well to thrombin, the absence of NOEs indicates that these side chains are not interacting back with the domain, and the backbone is more ordered. Thus, when NOEs from these essential hydrophobic side chains packed back against the domain are present, the backbone is less ordered. Conversely, when these side chains are exposed for binding, the backbone is more ordered. Preordering of the backbone of the binding site is consistent with the fact that the TM−thrombin interaction is entropically driven (*37*). It will be interesting to see how the backbone mobility of each of the domains changes upon binding to thrombin.

SUPPORTING INFORMATION AVAILABLE

One table giving fluorescence anisotrophy decay data. This material is available free of charge via the Internet at http://pubs.acs.org.

REFERENCES

1. Esmon, C. T. (2000) Regulation of blood coagulation, *Biochim. Biophys. Acta 1477*, 349−360.
2. Healy, A. M., Rayburn, H. B., Rosenberg, R. D., and Weiler, H. (1995) Absence of the blood-clotting regulator thrombomodulin causes embryonic lethality in mice before the development of a functional cardiovascular system, *Proc. Natl. Acad. Sci. U.S.A. 92*, 850−854.
3. Griffin, J. H., Ecatt, B., Zimmerman, T. S., Kleiss, A. J., and Widerman, C. (1981) Deficiency of protein C in congenital thrombotic disease, *J. Clin. Invest. 68*, 1370−1373.
4. White, C. E., Hunter, M. J., Meininger, D. P., White, L. R., and Komives, E. A. (1995) Large scale expression, purification and characterization of the smallest active fragment of thrombomodulin: the roles of the sixth domain and of methionine-388, *Protein Eng. 8*, 1177−1187.
5. Baerga-Ortiz, A., Rezaie, A. R., and Komives, E. A. (2000) Electrostatic dependence of the thrombin-thrombomodulin interaction, *J. Mol. Biol. 296*, 651−658.
6. Clarke, J. H., Light, D. R., Blasko, E., Parkinson, J. F., Nagashima, M., McLean, K., Vilander, L., Andrews, W. H., Morser, J., and Glaser, C. B. (1993) The short loop between epidermal growth factor-like domains 4 and 5 is critical for human thrombomodulin function, *J. Biol. Chem. 268*, 6309−6315.
7. Wood, M. J., Sampoli-Benitez, B. A., and Komives, E. A. (2000) Solution structure of the smallest cofactor-active fragment of thrombomodulin, *Nat. Struct. Biol. 7*, 200−204.
8. Fuentes-Prior, P., Iwanaga, Y., Huber, R., Pagila, R., Rumennik, G., Seto, M., Morser, J., Light, D. R., and Bode, W. (2000) Structural basis for the anticoagulant activity of the thrombin-thrombomodulin complex, *Nature 404*, 518−525.

9. Wood, M. J., Becvar, L. A., Prieto, J. H., Melacini, G., and Komives, E. A. (2003) NMR structures reveal how oxidation inactivates thrombomodulin, *Biochemistry 42*, 11932−11942.
10. Sampoli Benitez, B. A., Hunter, M. J., Meininger, D. P., and Komives, E. A. (1997) Structure of the fifth EGF-like domain of thrombomodulin: An EGF-like domain with a novel disulfide-bonding pattern, *J. Mol. Biol. 273*, 913−926.
11. Cavanagh, J., Fairbrother, W. J., Palmer, A. G., III, and Skelton, N. (1996) *Protein NMR Spectroscopy*, Academic Press, New York.
12. Ishima, R., and Torchia, D. A. (2000) Protein dynamics from NMR, *Nat. Struct. Biol. 7*, 740−743.
13. Kay, L. E., Muhandiram, D. R., Wolf, G., Shoelson, S. E., and Forman-Kay, J. D. (1998) Correlation between binding and dynamics at SH2 domain interfaces, *Nat. Struct. Biol. 5*, 156−163.
14. Palmer, A. G., III (1997) Probing molecular motion by NMR, *Curr. Opin. Struct. Biol. 7*, 732−737.
15. Melacini, G., Bonvin, A. M., Goodman, M., Boelens, R., and Kaptein, R. (2000) Hydration dynamics of the collagen triple helix by NMR, *J. Mol. Biol. 300*, 1041−1049.
16. Nooren, I. M. A., Rietveld, A. W. M., Melacini, G., Sauer, R. T., Kaptein, R., and Boelens, R. (1999) The solution structure and dynamics of an arc repressor mutant reveal premelting conformational changes related to DNA binding, *Biochemistry 38*, 6035−6042.
17. Zidek, L., Novotny, M. V., and Stone, M. J. (1999) Increased protein backbone conformational entropy upon hydrophobic ligand binding, *Nat. Struct. Biol. 6*, 1118−1121.
18. Yguerabide, J. (1972) Nanosecond fluorescence spectroscopy of macromolecules, *Methods Enzymol. 26* (Part C), 498−578.
19. Hauer, J. A., Taylor, S. S., and Johnson, D. A. (1999) Binding-dependent disorder−order transition in PKI alpha: a fluorescence anisotropy study, *Biochemistry 38*, 6774−6780.
20. Wang, S., Beechem, J. M., Gratton, E., and Glaser, M. (1991) Orientational distribution of 1,6-diphenyl-1,3,5-hexatriene in phospholipid vesicles as determined by global analysis of frequency domain fluorimetry data, *Biochemistry 30*, 5565−5572.
21. Hunter, M. J., and Komives, E. A. (1995) Thrombin-binding affinities of different disulfide-bonded isomers of the fifth EGF-like domain of thrombomodulin, *Protein Sci. 4*, 2129−2137.
22. Wood, M. J., and Komives, E. A. (1999) Production of large quantities of isotopically labeled protein in *Pichia pastoris* by fermentation, *J. Biomol. NMR 13*, 149−159.
23. Farrow, N. A., Muhandiram, R., Singer, A. U., Pascal, S. M., Kay, C. M., Gish, G., Shoelson, S. E., Pawson, T., Forman-Kay, J. D., and Kay, L. E. (1994) Backbone dynamics of a free and phosphopeptide-complexed Src homology 2 domain studied by ^{15}N NMR relaxation, *Biochemistry 33*, 5984−6003.
24. Markley, J. L., Horsley, W. J., and Klein, M. P. (1971) Spin−lattice relaxation measurements in slowly relaxing complex spectra, *J. Chem. Phys. 55*, 3604−3605.
25. Kroenke, C. D. J. P. L., Lee, L. K., Rance, M., and Palmer, A. G., III (1998) Longitudinal and transverse ^{1}H−^{15}N dipolar/^{15}N chemical shift anisotropy relaxation interference: Unambiguous Determination of rotational diffusion tensors and chemical exchange effects in biological macromolecules, *J. Am. Chem. Soc. 120*, 7905−7915.
26. Tjandra, N., Wingfield, P., Stahl, S., and Bax, A. (1996) Anisotropic rotational diffusion of perdeuterated HIV protease from ^{15}N NMR relaxation measurements at two magnetic fields, *J. Biomol. NMR 8*, 273−284.
27. Peng, J. W., and Wagner, G. (1992) Mapping of the spectral densities of N−H bond motions in eglin c using heteronuclear relaxation experiments, *Biochemistry 31*, 8571−8586.
28. Farrow, N. A., Zhang, O., Forman-Kay, J. D., and Kay, L. E. (1995) Comparison of the backbone dynamics of a folded and an unfolded SH3 domain existing in equilibrium in aqueous buffer, *Biochemistry 34*, 868−878.
29. Ishima, R., and Nagayama, K. (1995) Protein backbone dynamics revealed by quasi spectral density function analysis of amide N-15 nuclei, *Biochemistry 34*, 3162−3171.
30. Krishnan, V. V., Sukumar, M., Gierasch, L. M., and Cosman, M. (2000) Dynamics of cellular retinoic acid binding protein I on multiple time scales with implications for ligand binding, *Biochemistry 39*, 9119−9129.
31. Hiyama, Y., Niu, C. H., Silverton, J. V., Bavoso, A., and Torchia, D. A. (1988) Determination of N-15 chemical-shift tensor via N-15-H-2 dipolar coupling in Boc-glycylglycyl[N-15]glycine benzyl ester, *J. Am. Chem. Soc. 110*, 2378−2383.
32. Tjandra, N., Kuboniwa, H., Ren, H., and Bax, A. (1995) Rotational dynamics of calcium-free calmodulin studied by ^{15}N NMR relaxation measurements, *Eur. J. Biochem. 230*, 1014−1024.
33. Press, W. H. (1986) *Numerical recipes: the art of scientific computing*, Cambridge University Press, Cambridge and New York.
34. Mandel, A. M., Akke, M., and Palmer, A. G., III (1995) Backbone dynamics of *Escherichia coli* ribonuclease HI: Correlations with structure and function in an active enzyme, *J. Mol. Biol. 246*, 144−163.
35. Feher, V. A., and Cavanagh, J. (1999) Millisecond-timescale motions contribute to the function of the bacterial response regulator protein Spo0F, *Nature 400*, 289−293.
36. Nagashima, M., Lundh, E., Leonard, J. C., Morser, J., and Parkinson, J. F. (1993) Alanine-scanning mutagenesis of the epidermal growth factor-like domains of human thrombomodulin identifies critical residues for its cofactor activity, *J. Biol. Chem. 268*, 2888−2892.
37. Baerga-Ortiz, A., Bergqvist, S. P., Mandell, J. G., and Komives, E. A. (2004) Two different proteins that compete for binding to thrombin have opposite kinetic and thermodynamic profiles, *Protein Sci. 13*, 166−176.

BI0478852